Two-Dimensional Spatial Temperature and Density Measurements in an Arcjet Plasma Expanding through a Slit Nozzle*)

Kazuki KOZUE, Shogo NAKAMITSU, Shinichi NAMBA, Takuma ENDO, Ken TAKIYAMA, Kuninori SATO[1)] and Naoki TAMURA[1)]

Graduate School of Engineering, Hiroshima University, 1-4-1 Kagamiyama, Higashihiroshima, Hiroshima 739-8527, Japan
[1)]*National Institute for Fusion Science, 322-6 Oroshi-cho, Toki, Gifu 509-5292, Japan*

(Received 23 December 2010 / Accepted 17 February 2011)

To directly observe an arcjet inside the plasma discharge section, we developed an arcjet plasma device having a converging and diverging slit nozzle. Spectroscopic observations in the directions parallel and perpendicular to the plasma expansion axis were made to examine the characteristics of the arcjet plasma inside the nozzle. Intense continuum spectra due to bremsstrahlung were observed at visible and infrared wavelengths, from which the two-dimensional spatial distribution of the electron temperature was obtained. In addition, the electron density was determined by using the Stark broadening spectrum; the result indicated that high-density plasma was generated in the nozzle.

Keywords: arcjet plasma, plasma spectroscopy, atomic and molecular processes, electron temperature measurement, electron density measurement

DOI: 10.1585/pfr.6.2406054

1. Introduction

Arcjet plasmas have been applied in various scientific and engineering fields [1], such as material processing (welding and cutting) [2], chemical vapor deposition (CVD) [3], waste treatment [4], and plasma propulsion [5, 6]. For example, arcjet thrusters with a power range from several hundred watts to 100 kW have been developed for the main engine system of a spacecraft and the orbital and attitude control of a small satellite.

We have developed various arcjet plasma sources with axially symmetric structures [7]. High-density helium plasma expanding through an axisymmetric converging–diverging nozzle was observed by using a visible spectrometer to estimate the plasma parameters. An analysis of the continuum and line spectra showed that the electron temperature and density of the expanding plasma were 0.3 eV and 2.0×10^{15} cm^{-3}, respectively, at a position 45 mm from the nozzle exit [7]. However, in an axisymmetric device, the arc discharging section in which the thermal arc plasma is generated cannot be observed directly. Therefore, the temperature, density, and flow of the arcjet plasmas inside the nozzle are not well understood. Thus, to observe the plasma parameters, we developed an arcjet plasma device having a rectangular converging and diverging slit nozzle [8]. By observing the plasma emission, we successfully derived the electron temperature and density distribution on the expansion axis. Moreover, we found that the idealized continuum fluid model can be applied to the arcjet plasmas. However, the two-dimensional (2D) distributions of the electron temperature and density are essential for describing the plasma expansion behavior. Thus, in this study, the 2D characteristics of thermal arc plasmas inside the nozzle were examined spectroscopically.

2. Experimental Setup

We developed an arcjet plasma generator having a rectangular converging and diverging anode nozzle, allowing direct observation of the thermal arc plasma generated

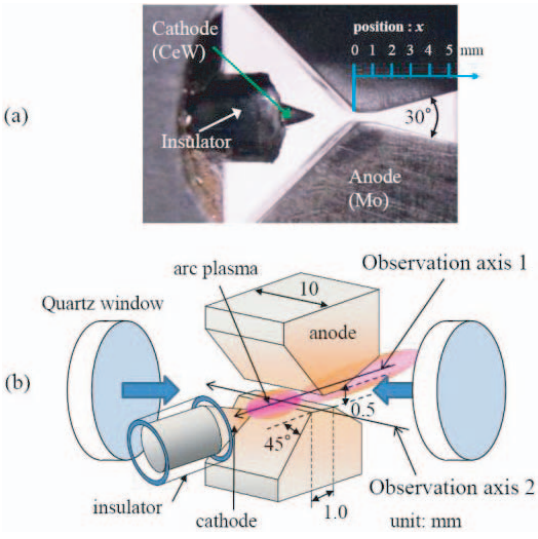

Fig. 1 Photograph (a) and schematic diagram (b) of the expanding arcjet plasma generator developed in this study.

author's e-mail: namba@hiroshima-u.ac.jp

*) This article is based on the presentation at the 20th International Toki Conference (ITC20).

inside the nozzle. Figures 1 (a) and (b) show a photograph and the schematic diagram of the expanding arcjet plasma generator, respectively. A pair of molybdenum anodes served as the converging and diverging slit nozzle; the separation between them was 0.5 mm. The cathode was a needle-shaped rod of cerium tungsten (CeW, ϕ = 2.4 mm). The throat (constrictor) width and length were 10.0 and 1.0 mm, respectively, and the diverging angle was 30°. An atmospheric thermal arc plasma was generated between the anode nozzle and the cathode. The gap length between the anode and cathode was around 1.0 mm. In this study, the discharge current and its voltage were 20 A and ~ 20 V, respectively, and the helium gas pressure was about 100 kPa in the discharge region (gas flow rate 12 L/min). Quartz windows were employed as the side walls to constrict lateral gas expansion.

A visible spectrometer with a focal length of 0.5 m was used to examine the characteristics of the expanding arcjet plasma The diffraction gratings were 150 grooves/mm for broadband emission measurement and 1200 grooves/mm for high-resolution measurement. The detector was a charge-coupled device camera with an image intensifier (ICCD camera). The emission was imaged by a lens onto the end of a bundled optical fiber with 48 cores. The light through the fiber was again imaged by a lens onto the entrance slit of the spectrometer. The spectral range observed using this system was λ = 400-750 nm. The 2D distribution of the plasma emission was obtained by moving the focus position onto the fiber by employing an optical stage. When the emission at wavelengths above 400 nm was measured, a sharp cut filter was used to block the second- and third-order spectra. The emission measurements were made in the directions parallel (observation axis 1) and perpendicular (axis 2) to the plasma expansion axis.

2D emission images were also observed using optical bandpass filters. The spatial resolution was around 13 μm. As described below, continuum radiation was emitted from the thermal arc plasma as well as atomic line spectra. To observe the continuum emission, we chose bandpass filters corresponding to λ = 532, 632, and 690 nm (bandwidth: ~ 10 nm), where no line emission appeared.

The spectral sensitivity for both emission measurements (spectrometer and bandpass filter) was calibrated by using standard lamps (tungsten ribbon and xenon discharge lamps).

3. Results and Discussion

Figure 2 shows typical emission spectra observed at x = 2 mm and y = 0 mm. Here the positions x and y were defined as the distances from the entrance of the nozzle throat and from the center of the paired anodes, respectively, as shown Fig. 1 (a). The discharge current was 20 A, and the diffraction grating employed was 150 grooves/mm. Intense continuum light spectra as well as line emission attributed to He I transitions were observed. The continuum spectra probably originated from bremsstrahlung radiation in the high-density plasma [8]; from these spectra, the electron temperature could be evaluated. The bremsstrahlung radiation $\varepsilon(\nu)$ is expressed as [9]

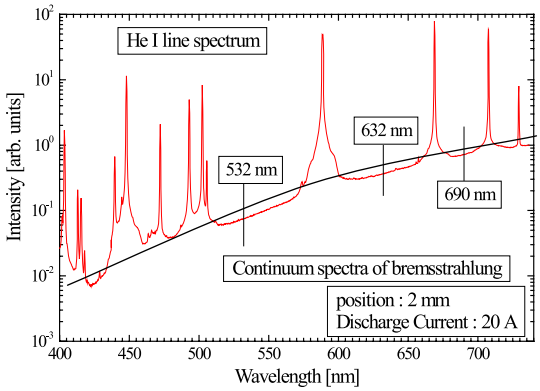

Fig. 2 Visible spectra emitted from He arcjet plasma. Measurement was made at x = 2 mm and y = 0 mm under a discharge current of 20 A and gas pressure of 100 kPa.

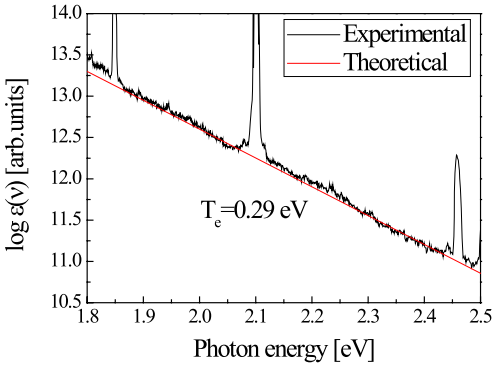

Fig. 3 Comparison of the experimental curve with that of bremsstrahlung radiation (T_e ~ 0.29 eV).

$$\varepsilon(\nu) = \frac{n_e}{4\pi}\frac{2^7}{(6\pi)^{3/2}}\left(\frac{m_e}{k_B T_e}\right)^{1/2}\frac{e^6}{c^3 m_e^2} \times \exp\left(-\frac{h\nu}{k_B T_e}\right)\sum_Z n_z Z^2 g_{ff}^z \quad (1)$$

where n_e is the electron density, T_e is the electron temperature, k_B is the Boltzmann constant, m_e is the electron mass, h is the Planck constant, Z is the charge number, n_z is the density of Z^+ ions, g_{ff}^z is the Gaunt factor for free–free transition, and the other notations have the usual meanings. Figure 3 shows the calibrated spectral intensity at x = 0 mm and y = 0 mm. Assuming that the electron temperature is 0.29 eV (~ 3,360 K), a good agreement between the experimental and theoretical curves was obtained. Figure 4 shows the 2D electron temperature distribution. The electron temperature inside the throat was determined to be 3,000-3,400 K, which was significantly lower than the values obtained by a numerical simulation (~ 10,000 K).

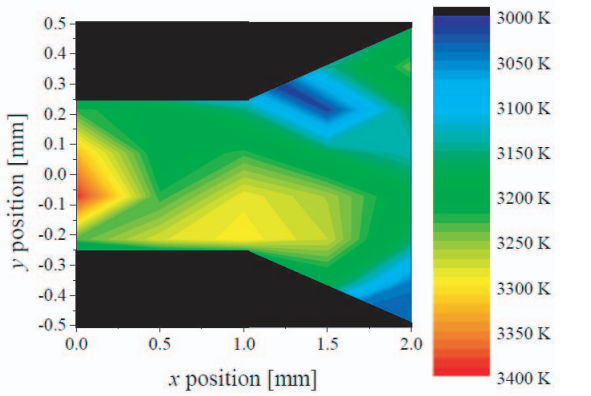

Fig. 4 Two-dimensional spatial distribution of the electron temperature obtained by analyzing the continuum spectra. Emission was measured using the spectrometer.

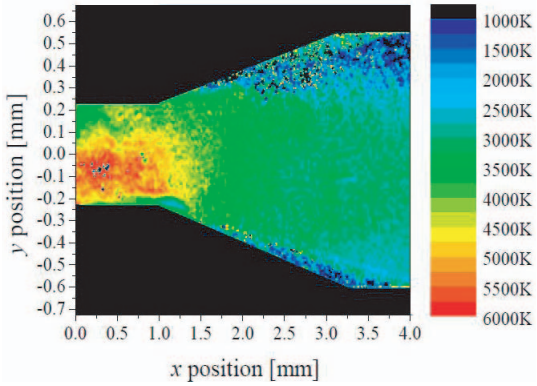

Fig. 5 2D electron temperature distribution obtained by analyzing the continuum spectra. Bandpass filters were used to derive the temperature.

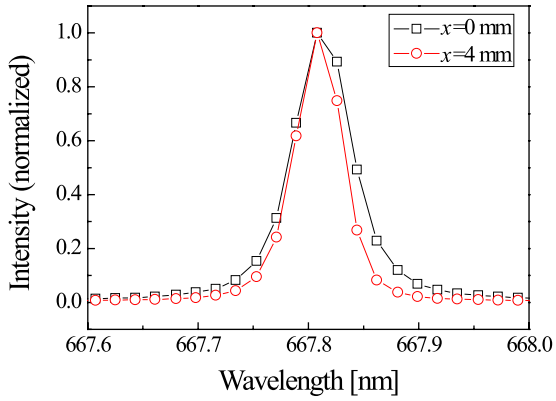

Fig. 6 Stark broadening spectra of He I 667 nm.

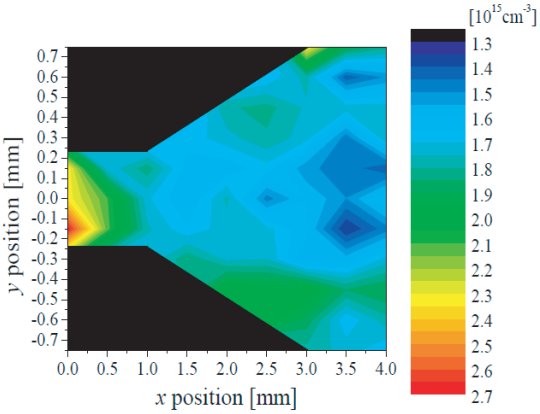

Fig. 7 2D electron density distribution determined by the Stark broadening spectrum of He I at 667.8 nm.

This implies that we cannot neglect the effect of the line-of-sight measurement along axis 2. In fact, He I (501.6 nm) line emission measured from axis 1 showed that the lateral length of the expanding plasma was around 5 mm.

Plasma emission at $\lambda = 532$, 632, and 690 nm was also measured by using bandpass filters. As described in the previous section, no distinct line emission was observed, as shown in Fig. 2. By the same procedure of temperature determination as that used for Fig. 3, we derived the 2D temperature distribution (Fig. 5). The temperature obtained by the bandpass filter was much higher than those in Fig. 4. The difference between them could be explained by temporal variations in the plasma emission during the measurements. Note that for spectrometer measurements, it took several minutes to obtain the 2D spatial distribution, whereas for the bandpass filter, only a minute or so was required. Observations using the bandpass filter, therefore, are likely to provide a favorable method of deriving the electron temperature.

On the other hand, the line spectra at $x = 0$ mm were obviously broadened, whereas the line profile became narrower as the distance from the cathode increased. Figure 6 shows the He I (667.8 nm) spectra at $x = 0$ and 4 mm ($y = 0$ mm). This variation in the spectral profile originated from Stark broadening, whose line width is described as a function of electron temperature and density [10]. Here, the line spectra observed can be expressed by the Voigt function, which is a convolution of Gaussian (Doppler and instrumental width) and Lorentzian (Stark broadening) line shapes. The Stark width $\Delta\lambda_s$ of atomic lines is approximately given by [9]

$$\Delta\lambda_s \approx 2\omega\left[1 + 1.75\times10^{-4} n_e^{1/4}\alpha \times\left(1 - 0.068 n_e^{1/6} T_e^{-1/2}\right)\right]\times10^{-16} n_e. \quad (2)$$

Here, n_e is the electron density (cm^{-3}), T_e is the electron temperature (K), ω is the full width at half maximum (FWHM) owing to electron impacts, and α is the ion broadening parameter. Since these variables depend on the temperature, we inferred them for various temperatures by using the values listed in reference 10. However, it is well known that the wing component of the spectral profile is dominated by the Lorentzian function. Therefore, the wing approximation was employed to determine the Stark width. The Lorentzian width of 667.8 nm (He $2p^1P$-$3d^1D$ transition) emission at $x = 0$ mm was $\Delta\lambda_s = 0.33$ nm (FWHM).

By substituting the temperature derived in Fig. 5 and the obtained Stark width into Eq. (2), the electron density was determined to be $\sim 2.0 \times 10^{15}\,\mathrm{cm}^{-3}$ at $x = 0$ mm. Figure 7 shows the 2D electron density distribution inside the anode nozzle, which indicates that high-density plasma was generated by the thermal arc discharge.

4. Summary

An arcjet plasma generator with a rectangular converging–diverging slit nozzle was constructed to directly observe the interior of the anode nozzle. The thermal arc plasma was characterized by spectroscopic observations. Intense continuum emission due to bremsstrahlung radiation was observed at visible and infrared wavelengths. From the spectral distribution, an electron temperature of 0.29 eV (~3,360 K) at the nozzle throat was derived. The emission was also measured using a bandpass filter to determine the temperature; the resulting temperatures were higher than those derived from spectroscopic observations. To determine the electron density, we analyzed the Stark broadening spectrum relevant to He atoms (667.8 nm). The density evaluated from the linewidth was as high as $\sim 2.0 \times 10^{15}\,\mathrm{cm}^{-3}$ at the throat.

[1] J. Reece Roth, *Industrial Plasma Engineering* (Taylor & Francis, 2001).
[2] M.I. Boulos, P. Fauchais and E. Pfender, *Thermal Plasmas, Fundamental and Applications* (Plenum, New York, 1994).
[3] D.M. Dobkin and M.K. Zuraw, *Principles of Chemical Vapor Deposition* (Kluwer Academic, 2003).
[4] J. Heberlein and A.B. Murphy, J. Phys. D: Appl. Phys. **41**, 053001 (2008).
[5] J.D. Anderson Jr., *Modern Compressible Flow with Historical Perspective*, 2nd ed. (McGraw Hill, New York, 1989).
[6] G.P. Sutton, *Rocket Propulsion Elements: Introduction to the Engineering of Rockets* (John Wiley & Sons, 1992).
[7] S. Namba, K. Nakamura, N. Yashio, S. Furukawa, K. Takiyama and K. Sato, J. Plasma Fusion Res. **8**, 1348 (2009).
[8] S. Namba, N. Yashio, K. Kozue, K. Nakamura, T. Endo, K. Takiyama and K. Sato, Jpn. J. Appl. Phys. **48**, 116005 (2009).
[9] R.H. Huddlestone and S.L. Leonard, *Plasma Diagnostic Techniques*, eds. (Academic, New York, 1965).
[10] H.R. Griem *Spectral Line Broadening by Plasmas* (Academic, New York, 1974).